Solution Structure of Human Apolipoprotein(a) Kringle IV Type 6[†,‡]

Bernhard Maderegger,[§] Wolfgang Bermel,[∥] Andelko Hrzenjak,[⊥] Gert M. Kostner,[⊥] and Heinz Sterk*[,§]

Institute of Chemistry, Karl Franzens University Graz, Heinrichstrasse 28, A-8010 Graz, Austria, Bruker Analytik GMBH, Silberstreifen, Rheinstetten/Karlsruhe, Germany, and Institute of Medical Biochemistry and Medical Molecular Biology, Karl Franzens University Graz, Harrachgasse 21, A-8010 Graz, Austria

Received July 9, 2001; Revised Manuscript Received October 26, 2001

ABSTRACT: The structure of apo(a) KIVT6 was investigated by two- and three-dimensional homo- and heteronuclear NMR spectroscopy. The solution structure of apo(a) KIVT6 contains only a small amount of regular secondary structure elements, comprising a short piece of antiparallel β-sheet formed by residues Trp62−Tyr64 and Trp72−Tyr74, a short piece of parallel β-sheet formed by the residues Cys1−Tyr2 and Thr78−Gln79, and a small 3_{10}-helix within residues Thr38−Tyr40. The backbone as well as the side chains are arranged in a way similar to those of apo(a) KIVT7, apo(a) KIVT10, and plasminogen K4. We determined additionally the K_d value of 0.31 ± 0.04 mM for the binding of ϵ-aminocaproic acid (EACA) to apo(a) KIVT6 and mapped the binding region on apo(a) KIVT6 by means of chemical shift perturbation. This lysine binding activity, which was reported to occur within apo(a) KIVT5−8, is functionally different from the lysine binding activity found for apo(a) KIVT10.

Lipoprotein (a) [Lp(a)][1] is a LDL-like particle in human plasma, which was first described by Berg in 1963 (*1*). Although this happened nearly 40 years ago, the physiological function of Lp(a) is still unknown (*2*). Chemically, Lp(a) consists of the large glycoprotein apo(a), which is covalently linked to the apoB-100 moiety of LDL through a single disulfide bridge. Apo(a) contains a multiple kringle domain and a catalytically inactive serine protease domain (*3*). The apo(a) gene has evolved from the plasminogen gene by gene duplication (*4*). The multiple kringle domain of apo(a) lacks the plasminogen kringles 1−3 and comprises 14−37 plasminogen K4-like repeats, which are classified in 10 subtypes denoted as apo(a) KIVT1−KIVT10, and a single plasminogen K5-like domain. The apo(a) KIVT1−10 share 75−94% sequence homology with plasminogen K4 (*3*). Apo(a) KIVT1 and apo(a) KIVT3−10 are present in single copies in apo(a), whereas apo(a) KIVT2 exists in up to 40 or more copies and is responsible for the considerable size polymorphism of apo(a).

Kringles are autonomous folding units and consist of a single polypeptide chain with a length of approximately 80 amino acids. They exhibit a characteristic disulfide linkage pattern of six cysteine residues, which are joined in a 1−6, 2−4, and 3−5 manner (*5*, *6*). Different numbers of kringle domains have been found in several other plasma proteins, including prothrombin (*6*), factor XII (*7*), tissue-type and urokinase-type plasminogen activator (*8*, *9*), and hepatocyte growth factor (*10*). In all cases the two inner cystine bridges (2−4 and 3−5) maintain the stability of the kringle fold (*11*).

In vitro assembling studies of LDL with different recombinant apo(a) constructs revealed that apo(a) KIVT6 and apo(a) KIVT7 have a crucial impact on Lp(a) assembly (*12*−*14*). This region on apo(a) seems to be also important in other protein−protein binding interactions, such as the recognition of Lp(a) and apo(a) by the macrophage Lp(a)/apo(a) receptor (*15*) or the binding of free apo(a) to plasminogen-treated fibrinogen (*16*). These interactions are, however, suppressed upon the addition of lysine or lysine analogous compounds, which bind to kringle domains via a well-conserved lysine binding site (LBS). Two functionally distinct lysine binding site types have been identified in apo(a) (*17*). The first type represents a high-affinity binding site and is only present in apo(a) KIVT10 (*18*). The second type of LBS in apo(a) is existent in apo(a) KIVT6 (*19*) and in apo(a) KIVT7 (*20*); it represents a binding site with moderate activity.

In this study we provide a detailed solution structure model for apo(a) KIVT6, showing a high degree of similarity to the X-ray structures of apo(a) KIVT7 (*20*), apo(a) KIVT10 (*21*), and plasminogen K4 (*22*−*24*) but also some important differences. We will demonstrate further that binding of EACA to apo(a) KIVT6 is based on the same residues which are responsible for the binding of EACA to apo(a) KIVT10

[†] This research was supported by the Fonds zur Förderung der wissenschaftlichen Forschung, project numbers 12881CHE and SFB F702.

[‡] PDB ID 1JFN, RCSB ID 013714, and BMRB ID 5075.

* To whom correspondence should be addressed. Phone: 00433163805326. Fax: 00433163809840. E-mail: heinz.sterk@kfunigraz.ac.at.

[§] Institute of Chemistry, Karl Franzens University Graz.

[∥] Bruker Analytik GMBH.

[⊥] Institute of Medical Biochemistry and Medical Molecular Biology, Karl Franzens University Graz.

[1] Abbreviations: apo(a), apolipoprotein (a); apoB, apolipoprotein B; AMCHA, *trans*-(aminomethyl)cyclohexanecarboxylic acid; EACA, ϵ-aminocaproic acid; apo(a) KIVT1−10, apo(a) kringle types 1−10; LBS, lysine binding site; LDL, low-density lipoprotein; Lp(a), lipoprotein (a); MALDI-TOF, matrix-assisted laser desorption time-of-flight mass spectrometer; RP-HPLC, reversed-phase high-pressure liquid chromatography; HSQC, heteronuclear single-quantum coherence; HNHA, *J* correlation between the NH and H_α proton; TOCSY, total correlation spectroscopy; NOE, nuclear Overhauser effect; NOESY, nuclear Overhauser spectroscopy; TPPI, time-proportional phase incrementation; SDS−PAGE, sodium dodecyl sulfate−polyacrylamide gel electrophoresis. Standard abbreviations are used for the common amino acids.

10.1021/bi011430k CCC: $22.00
Published on Web 12/18/2001

and plasminogen K4. The structure model presented may serve as a starting point for the design of a selective ligand for apo(a) KIVT6. Such a selective ligand would be a versatile tool to further elucidate protein−kringle interactions mediated by apo(a) KIVT6 and might serve as a lead structure for the development of anti-hyperlipoprotein(a) drugs, facilitating the clinical control of Lp(a) plasma levels.

MATERIALS AND METHODS

Preparation of Apo(a) KIVT6. Recombinant apo(a) KIVT6 was expressed, purified, and refolded as described previously (*19*), except for the following changes. The *Escherichia coli* cultures for the preparation of the isotopically labeled apo(a) KIVT6 sample were grown in a mixture consisting of 50% M9 minimal medium and 50% Celtone medium (Martek Stable Isotopes) with the appropriate isotope labeling. After binding of refolded apo(a) KIVT6 to lysine−Sepharose, only a brief washing with 0.1 M NaCl and 30 mM Tris-HCl, pH 8.0, was performed. Bound apo(a) KIVT6 was eluted with 0.2 M NaCl and 30 mM Tris-HCl, pH 8.0. Fractions containing nearly pure protein were further purified by using TALON metal affinity resin according to the protocol supplied by the manufacturer. The eluated fractions from the metal affinity column, obtained with a 50 mM histidine, 100 mM NaCl, 10 mM Tris-HCl, pH 8.0, buffer were additionally purified by RP-HPLC. The RP-HPLC chromatography was carried out on a Shimadzu LC-10 VP liquid chromatograph equipped with a 125 × 4 mm Vydac 218 TPB RP-18 column. Elution from the RP-HPLC was maintained at constant temperature with a linear gradient of acetonitrile in water, varying from 10% to 90% acetonitrile in 30 min. Both solvents were supplemented with 0.1% TFA. Efflux absorbance was monitored at 215 and 280 nm. The final protein concentration in the NMR samples was 0.7 mM in 15 mM sodium phosphate and 50 mM NaCl, pH 6.5, supplemented with 10% D_2O. Protein concentrations were determined with a Bradford microassay procedure (Bio-Rad). The purity of the apo(a) KIVT6 samples was assayed by SDS−PAGE electrophoresis with Coomassie blue R-250 staining according to standard procedures. In the final product no impurity was detectable. NMR experiments were performed with 300 μL of the above solution in a 5 mm sealed microcell (Shigemi Co.).

Physical Characterization and NMR Spectroscopy. Physical characterization of apo(a) KIVT6 was accomplished by mass spectroscopy. Purified apo(a) KIVT6 protein was analyzed on a Kratos Kompact 2 MALDI-TOF mass spectrometer. Circular dichroism spectroscopy was carried out on a Jobin Ivon spectropolarimeter with an unlabeled apo(a) KIVT6 sample. The protein concentration was 1 mg/mL in 100 mM NaCl and 20 mM sodium phosphate at pH 7.4. Analysis of the CD spectra was best described with an unconstrained least-squares fit according to the Bolotina model (*25*). Multidimensional spectra were collected on a Bruker Avance 600 MHz spectrometer using a 5 mm triple resonance probe. Experiments were carried out with a sample temperature of 303 K. In the case of ^1H spectra the WATERGATE technique was used for water suppression. Phase sensitivity in the indirect dimensions was achieved by the States−TPPI method (*26*). ^1H chemical shift referencing was performed by using the HDO resonance line, with appropriate corrections for the pH and temperature shifts. The ^{15}N and ^{13}C chemical shifts were determined indirectly according to the gyromagnetic ratios (*27*). Sequential backbone assignments were derived from HNCO (*28*−*30*), HNCA (*28*, *30*), HNCOCA (*28*, *30*), and CBCACONH (*28*, *31*) triple resonance spectra. Side chain assignments were achieved from 3D $^1H-^{15}N$ TOCSY-HSQC, aromatic ^{13}C HCCH-TOCSY, and ^{13}C HCCH-TOCSY (*32*) experiments. NOE cross-peaks were extracted from 3D $^1H-^{13}C$ NOESY-HSQC and 3D aromatic $^1H-^{13}C$ NOESY-HSQC as well as from 3D $^1H-^{15}N$ NOESY-HSQC (*33*−*35*) spectra, all with a mixing time of 150 ms. $^3J_{HN\alpha}$ coupling constants were derived from a 3D HNHA experiment (*36*). $^1H-^2D$ exchange kinetics of backbone amide protons were monitored by recording a series of $^1H-^{15}N$ HSQC spectra at various times after the sample was dissolved in D_2O containing 15 mM sodium phosphate and 50 mM NaCl, pH 6.5. The first measurement averages over half an hour; visible signals are marked with medium (m); the second measurement [slow (s)] shows the unexchanged backbone proton after 2.5 h. The final measurement was done after 14 h; the unexchanged signals are marked with (ss). Spectral processing of the acquired FID's was performed on a Silicon Graphics O2 R5000 workstation by employing the NMRPipe Software (*37*). Indirect dimensions were generally zero filled, and linear prediction algorithms were applied when further improvement of the digital resolution was necessary. Spectra were assigned and integrated by using the ANSIG software (*38*, *39*). The titration experiments were carried out by recording a series of 2D $^1H-^{15}N$ HSQC experiments in the presence of increasing amounts of unlabeled EACA. The EACA was added in small volume increments from a 50 mM stock solution, prepared in the same buffer as the protein sample, to ensure constant buffer conditions during the titration.

Distance Restraints and Structure Calculation. The interproton distance restraints were derived by categorization of NOE cross-peaks into three classes (weak, medium, and strong) according to their integrated volumes (*40*). The integrated volumes for NOE cross-peaks involving methyl groups were reduced to one-third. The upper bounds for the distance restraints were set to 2.7 Å for the strong class NOE cross-peaks, 3.6 Å for the medium class, and 5.0 Å for the weak class (*41*). The lower bounds were set to 1.8 Å in all three classes. Pseudoatom corrections for nonstereospecifically assigned diastereotopic protons were applied (*42*). Dihedral angle restraints for ϕ angles were calculated from $^3J_{HN\alpha}$ coupling constants (*43*), revealed by a 3D HNHA experiment. Values for $^3J_{HN\alpha} < 5.0$ Hz were correlated with ϕ angles of $-60 \pm 30°$, values of 5−8 Hz with $-105 \pm 55°$, values of 8−9 Hz with $-120 \pm 40°$, and values >9 Hz with $-120 \pm 30°$. Additional dihedral restraints for ϕ and ψ angles were established with the program TALOS on the basis of the ^1H, ^{15}N, $^{13}C\alpha$, $^{13}C\beta$, and ^{13}CO chemical shifts (*44*). Only those restraints which were classified by the program as good were added to the structure calculation. Structure calculations were performed with the program X-PLOR Version 3.0 (*45*) on a Silicon Graphics O2 R5000 workstation. The CHARMM (*46*) field with a standard parametrization, including NOE pseudoenergy, was employed. The initial template structure was a randomized extended strand conformation, containing no disulfide bridges. On the basis of the high degree of homology of already

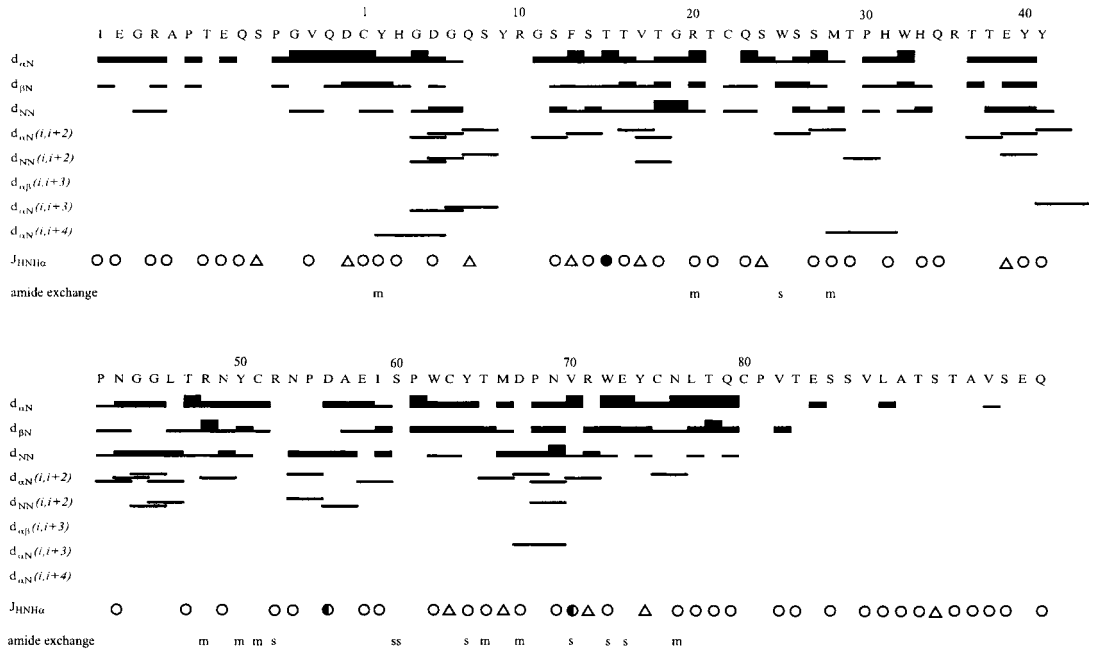

FIGURE 1: Summary of the sequential NOE connectivities and $^3J_{HNH\alpha}$ coupling constants observed for apo(a) KIVT6. The heights of the bars reflect the intensity class of the NOE cross-peaks (strong, medium, and weak). $^3J_{HNH\alpha}$ values <5 Hz are indicated by triangles, values of 5−8 Hz are indicated by circles, values of 8−9 Hz are indicated by half-filled circles, and values >9 Hz are indicated by filled circles. Amide exchange after dissolving in D_2O is classified as being of medium (m), slow (s), and very slow (ss) exchange rates, respectively.

known kringle structures and the striking conservation of the disulfide bridge linkage pattern in all those structures, disulfide bridges in our calculations were introduced in accordance with these kringle folds. In the first step of structure calculation a distance geometry algorithm was applied to the backbone atoms of the protein. After these substructures were embedded, a distance geometry/simulated annealing hybrid protocol (*47*) was followed by a simulated annealing refinement protocol in vacuo.

RESULTS

MS, CD, and NMR Spectroscopy. As apo(a) KIVT6 was expressed with its full-length interkringle linker sequences and an additional His tag on the N-terminal end, the residue numbering differs from other studies. Residues Cys1−Cys80 in the original kringle numbering convention correspond to Cys25−Cys102 in our expressed full-length protein. Residues Ala1−Asp24 and Pro103−Gln119 correspond to the N-terminal and C-terminal interkringle linker sequence. To make the comparison with other kringle studies easier, according to the suggestion of a referee, the mentioned N- and C-terminal peptide links will be omitted for the discussion and the numbering of the residues will follow the standard kringle numbering convention. Amino acid numbers in brackets [*x*] refer to our expressed full-length protein. The N-terminal methionine was not taken into account because it was removed in the majority of apo(a) KIVT6 molecules as predicted by the N-end rule. Experimental evidence supporting this prediction is given by MALDI-TOF mass spectrometry, which revealed masses of 13719 Da for the ^{15}N-labeled and 14312 kDa for the ^{13}C/^{15}N-double-labeled apo(a) KIVT6 sample. Taking into account the resolution of the mass spectrometer, both of these masses are in conformity with the calculated molecular masses of 13748 and 14323 Da, when the removal of the N-terminal methionine is considered. CD spectra recorded from a 1 mM unlabeled apo(a) KIVT6 solution in 150 mM phosphate-buffered saline exhibit an unusual molar ellipticity graph, which is commonly observed in kringle domains with a negative ellipticity peak at 200 nm and a positive ellipticity peak at 230 nm. Unconstrained analysis of the CD spectrum was done by a least-squares fit with various models [e.g., Greenfield et al. (*48*), Chen et al. (*49*), Yang et al. (*50*), and Bolotina et al. (*25*)]. Thereby, it turned out that the model of Bolotina reflects best the positive ellipticity peak at 230 nm. We obtained a relative content of 3% α-helix, 18% *β*-sheet, 54% turn, and 25% coil conformation.

The backbone amide resonances of residues 1−9, corresponding to the first three ^{15}N-terminal amino acids from the polylinker and six histidine residues from the His tag, as well as Ser8, Arg10, Arg35, and Thr37, could not be located unambiguously in the ^{1}H−^{15}N HSQC spectra. From the remaining 105 residues sequence-specific assignments from 97% of the backbone resonances and over 90% of the side chain resonances were obtained. The $^{13}C\gamma$ and $^{13}C\delta$ side chain resonances of residues Glu[11]−Gln[23] and Pro[103]−Gln[119] could not be resolved due to severe chemical shift overlap. However, their ^{13}C chemical shifts are most probably close to the random coil shift value as suggested by the intense signal observed near the random coil shift position and by the fact that none of the resolved ^{1}H chemical shifts of these residues show a large deviation from the random coil chemical shift value. The ^{1}H resonances of the hydroxyl group of Thr15 and Thr65 were identified by an unambiguous NOE pattern. The large downfield shift of these protons is indicating an involvement in a strong hydrogen-bonding interaction. Similar downfield shifts for the ^{1}H resonances of the hydroxyl group have been reported for the corresponding threonine residues in human (*24*) and equine (*22*) plasminogen K4.

A total number of 938 nontrivial interproton distance restraints were derived from the mentioned NOE spectra

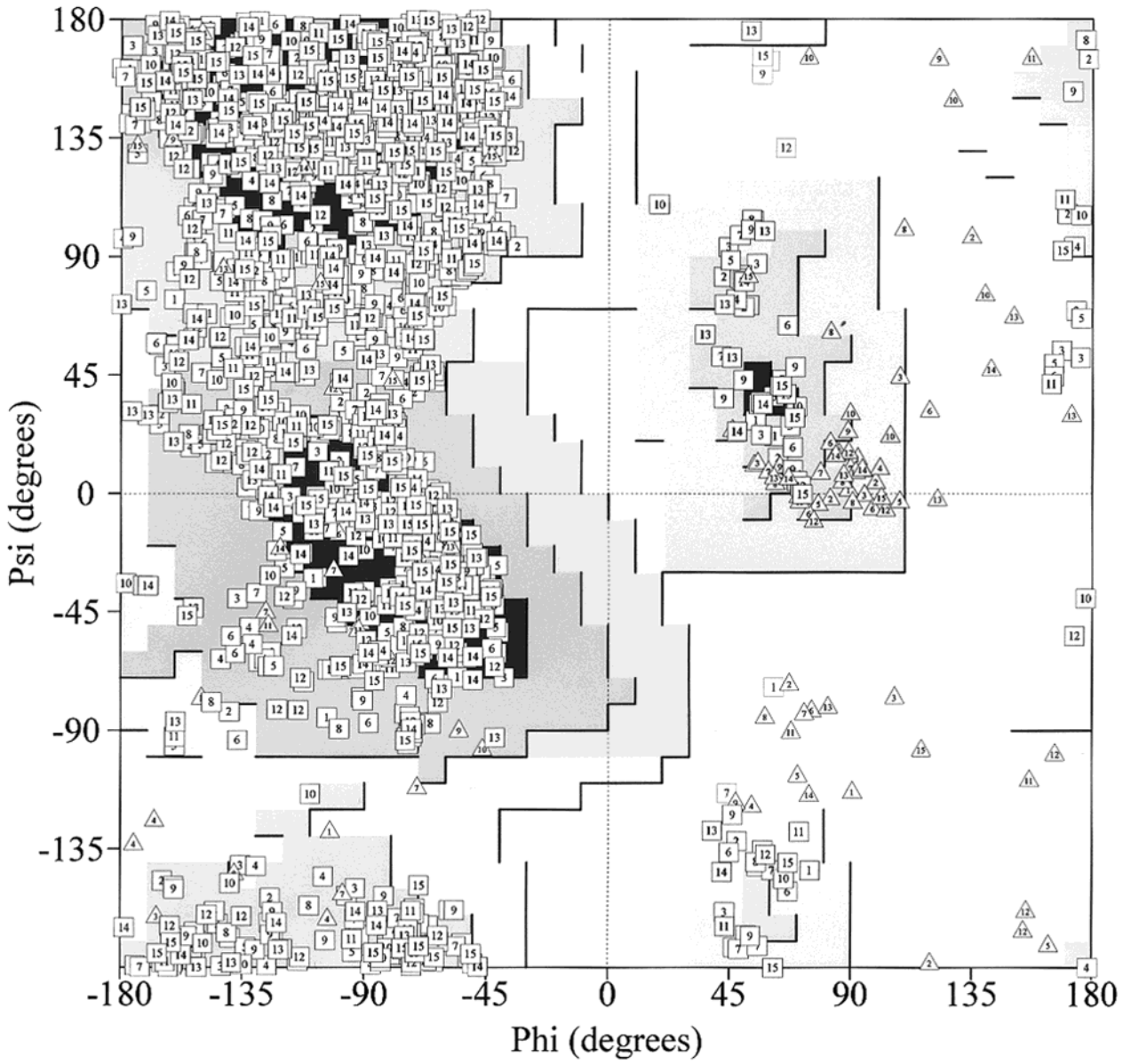

FIGURE 2: Ramachandran plot indicating the distribution of the backbone dihedral angles ϕ and ψ of the final 15 lowest energy structures calculated by X-PLOR. The Gly residues are represented by triangles. The figure was created with PROCHECK (*72*).

encompassing 292 intraresidue, 273 sequential, 140 short range ($|i - j| = 2-4$), and 233 long range. A summary of the observed sequential NOE connectivities for apo(a) KIVT6 is shown in Figure 1. The motional behavior of apo(a) KIVT6 is reflected by the number of extractable interproton distance restraints from the NOESY spectra. Thereby, two major regions of apo(a) KIVT6 can be distinguished. In the interkringle region, which forms the N-terminal and C-terminal ends of apo(a) KIVT6 and comprises residues Ala-[2]−Asp[24] and Pro[103]−Gln[119], only 48 intraresidue and 38 sequential distance restraints could be established. This corresponds to no more than 2.1 restraints/residue, in sharp contrast to the central part, i.e., the kringle domain itself, ranging from Cys1 to Cys80, for which an average of 10.9 restraints/residue could be established. Interproton distance restraints were supplemented by 70 torsion angle restraints for ϕ and 12 torsion angle restraints for ψ angles, established by the measurement of $^3J_{HNH\alpha}$ coupling constants and empirically derived on the basis of the ^{1}H, ^{15}N, ^{13}Cα, ^{13}Cβ, and ^{13}CO chemical shifts by the use of the TALOS program. The exchange experiment shows that in the neighborhood of the disulfide bridges as well as in the area of the β-sheets the exchange rate is reduced. The majority of the slow-exchange hydrogen bonds is located in the C-terminal half, between residues Arg48−Asn76. The structure calculations reflect this by a significant smaller rmsd for the backbone heavy atoms of the C-terminal half (0.692 versus 0.887 Å for the N-terminal half).

Solution Structure of Apo(a) KIVT6. From a final family of 150 refined structures, a subset of 15 structures, exhibiting the lowest total energies (including NOE pseudoenergy and simulated annealing in vacuo), was extracted for the final structural analysis and presentation. None of these structures had a NOE distance violation greater than 0.5 Å or a dihedral angle violation of more than 5°. A total of 53.3% of the residues were in the most favored region of the Ramachandran plot (see Figure 2), 41.9% were in the additionally allowed region, 4.4% were in the generously allowed region, and 0.4% were in the disallowed region. The interkringle regions were found to be conformationally unstructured as

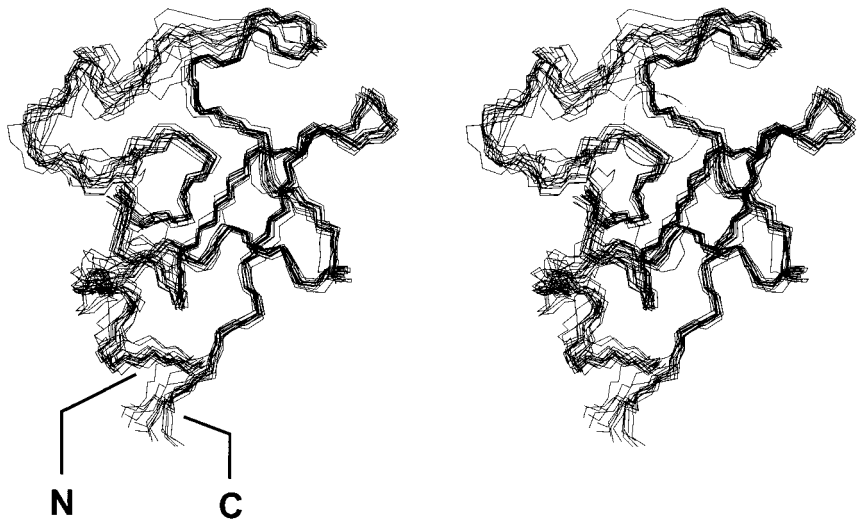

FIGURE 3: Stereoview of the backbone superimposition of the 15 final structures of apo(a) KIVT6 with lowest energy. Residues Cys1−Cys80 are depicted. The N and C termini are labeled. The Cα atoms were used for superposition. This figure and all other molecular graphs were created with MOLMOL (*73*).

Table 1: Structural Statistics for 15 Selected Apo(a) KIVT6 Structures

total no. of constraints	938
intraresidue	292
sequential ($i - j = 1$)	273
medium range ($1 < i - j < 4$)	140
long range ($i - j > 4$)	233
dihedral constraints	92
mean values of restraint violations	
NOE violations >0.3 (Å)	1.3
dihedral angle violations >3 (deg)	1.0
Ramachandran plot distribution	
residues in most favored region (%)	53.3
residues in allowed region (%)	41.9
residues in generously allowed region (%)	4.4
residues in disallowed region (%)	0.4
rmsd from idealized geometry	
bonds (Å)	0.0025 ± 0.00001
angles (Å)	0.547 ± 0.010
improper (Å)	0.391 ± 0.007
X-PLOR energy	
total (kcal/mol)	267.3 ± 22.1
bond (kcal/mol)	11.9 ± 0.8
angle (kcal/mol)	149.3 ± 5.2
improper (kcal/mol)	24.1 ± 0.8
vdw (kcal/mol)	20.5 ± 3.8
NOE (kcal/mol)	48.9 ± 7.5
dihedral (kcal/mol)	12.7 ± 17.8
rmsd from mean structure	
backbone [residues 25−102 (Å)]	0.841
heavy atoms [residues 25−102 (Å)]	1.312

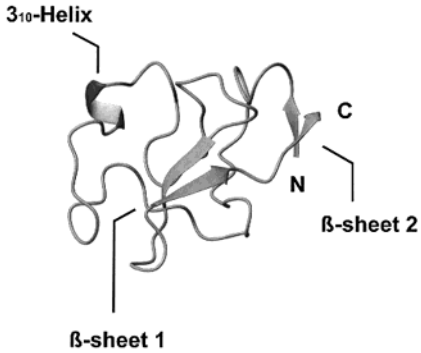

FIGURE 4: Ribbon diagram of the closest to the mean structure of apo(a) KIVT6. Residues Cys1−Cys80 are depicted. Secondary elements and N and C termini are labeled.

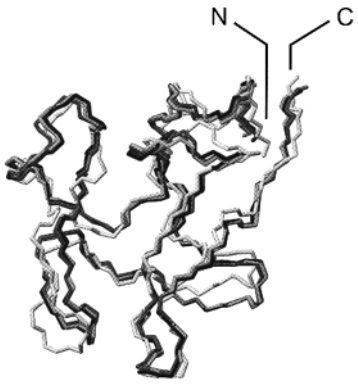

FIGURE 5: Structural comparison of the backbone folding of apo(a) KIVT6 (light gray), apo(a) KIVT7 (medium gray), apo(a) KIVT10 (dark gray), and plasminogen K4 (black). The Cα atoms were used for superposition.

expected by the low number of NOEs observed in this part of apo(a) KIVT6. Therefore, these regions were omitted in the graphical representation of the structure ensemble in Figure 3 and in the calculation of rmsd values. In Figure 3 a superposition of the backbone polypeptide chains of these 15 lowest total energy structures, fitted to the arithmetic mean structure, is depicted. The structural statistics of the solution structure of apo(a) KIVT6 are summarized in Table 1. As indicated by a rsmd of 0.841 Å for the backbone heavy atoms and of 1.312 Å for all heavy atoms, the backbone and also most of the side chains of apo(a) KIVT6 are found to be well-defined. A ribbon drawing of the closest to mean structure of apo(a) KIVT6 is shown in Figure 4. The secondary structure of apo(a) KIVT6 is mainly composed of several loops and turns separated by sequence parts, which exhibit a coil conformation. A small piece of an antiparallel β-sheet comprising residues Trp62−Tyr64 and Trp72−Tyr74 has been identified. A further small β-sheet, with parallel strands, is formed by residues Cys1−Tyr2 and Thr78−Gln79. In a small region spanning residues Thr38−Tyr40 a 3_{10}-helix is present in apo(a) KIVT6. This result is similar to the urokinase-type plasminogen activator (*51*), the plasminogen K1−AMCHA complex (*52*), plasminogen K2 (*53*),

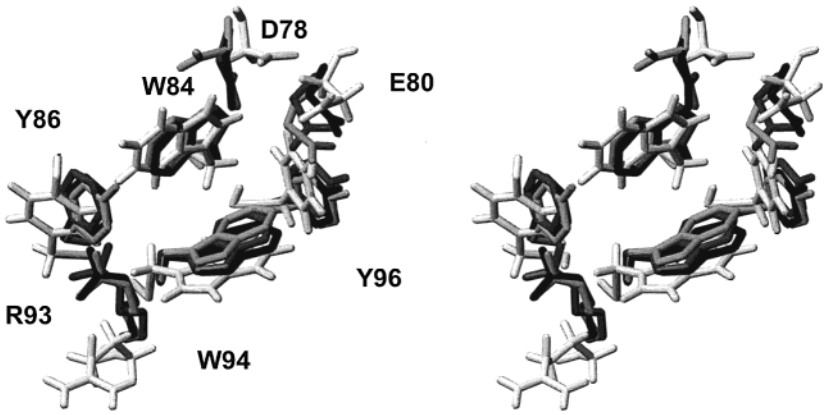

FIGURE 6: Structural comparison of the lysine binding sites of apo(a) KIVT6 (light gray), apo(a) KIVT7 (medium gray), apo(a) KIVT10 (dark gray), and plasminogen K4 (black). The backbone heavy atoms of the indicated residues were used for superposition.

and the tissue-type plasminogen activator K2 (*54*) which also contain small helices, whereas in apo(a) KIVT10 (*21*) and plasminogen K4 (*22*−*24*) helices are completely absent. This major turn and coil structure, with a low content of β-sheet and a very low helical content, is in line with the secondary structure elements identified in the CD spectrum of apo(a) KIVT6.

Comparison to X-ray Structures. Apo(a) KIVT7, apo(a) KIVT10, and plasminogen K4 represent the closest homologous protein domains to apo(a) KIVT6 for which a three-dimensional structure has been determined. Figure 5 shows the overlay of the closest to average structure of apo(a) KIVT6 and the crystal structures of apo(a) KIVT7 (*20*), apo(a) KIVT10 (*21*), and plasminogen K4 (*23*). The rmsd values for superposition of the Cα traces of apo(a) KIVT6 with apo(a) KIVT7, apo(a) KIVT10, and plasminogen K4 were found to be 1.65, 1.50, and 1.64 Å, respectively, which corresponds to a very similar backbone folding. Analysis of the side chain orientations revealed that the majority of the side chains possesses similar positions as in apo(a) KIVT7, apo(a) KIVT10, and plasminogen K4. This statement holds for conserved as well as for not conserved residues with very few exceptions. Within the LBS region of apo(a) KIVT6 the side chain of Arg71 was found to have the largest deviation from the corresponding position in apo(a) KIVT7, apo(a) KIVT10, and plasminogen K4 (see Figure 6). Also, the side chain of Thr65 is rotated by a χ_1 angle of approximately 180°. Thereby, the methyl group and the hydroxyl group of Thr65 are placed in their opposite positions compared to apo(a) KIVT10 and plasminogen K4. However, this different side chain orientation should only have minor functional consequences as a Thr → Met mutation of the corresponding residue in apo(a) KIVT10 had no structural impact on the lysine binding function (*55*). A further notable result is the orientation of the hydrophobic Trp32. From our measurements we can conclude that Trp32 is orientated outside toward the solvent and thereby has no influence on the backbone folding of apo(a) KIVT6.

Binding of EACA to Apo(a) KIVT6. On the basis of the high degree of homology with apo(a) KIVT10 and plasminogen K4, both of which have been demonstrated to interact with EACA and other lysine analogous substances, the existence of an LBS within apo(a) KIVT6 has been predicted (*18*). This lysine binding function was recently proven by binding studies (*19*). We investigated the interaction between EACA and apo(a) KIVT6 by chemical shift perturbation mapping on a series of $^1H-^{15}N$ HSQC spectra acquired with increasing amounts of EACA in the sample; a hyperbolic fit was applied to the data points using the program xcrvfit (*56*) in order to the determinate K_d value. A graph of one hyperbolic fit is shown in the insets of Figure 7 and revealed a K_d value of 310 ± 40 μM for the binding of EACA to apo(a) KIVT6. Comparison of this result with previously determined K_d values for the binding of EACA to various kringle domains indicates an intermediate affinity of EACA to KIVT6. For example, K_d values are found to be 20 μM for apo(a) KIVT10, 12−15 μM for plasminogen K1 (*57*−*59*), 410−430 μM for plasminogen K2 (*57*, *60*), 26−50 μM for plasminogen K4 (*61*−*63*), 100−140 μM for plasminogen K5 (*61*, *64*, *65*), and 46−52 μM for tissue-type plasminogen activator K2 (*66*, *67*). The overlaid $^1H-^{15}N$ HSQC spectra are depicted in Figure 7. Chemical shift perturbations were observed for 22 residues; thereby Asp55, Glu57, and Ile58 exhibited the largest differences. Analysis of the chemical shift perturbation pattern obtained from the HSQC spectra of apo(a) KIVT6 revealed for the LBS a more or less pronounced homology for apo(a) KIVT10 (*55*), plasminogen K1 (*52*, *68*), K2 (*53*), K4 (*22*, *24*, *69*), and K5 (*64*, *65*), as well as tissue-type plasminogen activator K2 (*54*, *67*, *70*). All residues, for which a chemical shift difference was observed, have positions within or adjacent to the LBS. Thereby the anionic center of the LBS in apo(a) KIVT6 consisting of Asp55 and Glu57 is separated from a cationic center consisting of Arg71 by a hydrophobic channel. This hydrophobic channel is formed by the residues Trp62, Tyr64, Trp72, and Tyr74. Therefore, these data clearly indicate that binding of EACA to apo(a) KIVT6 occurs in a manner similar to that reported for apo(a) KIVT10 and plasminogen K1, K2, K4, and K5, as well as tissue-type plasminogen activator K2.

DISCUSSION

In this report we present the first solution structure of an apo(a) kringle domain comprising a type 2 LBS and provide evidence that binding of the lysine analogous compound EACA to apo(a) KIVT6 is mediated via this LBS. The structure of apo(a) KIVT6 consists largely of an arrangement of loops and turns with small pieces of an antiparallel and parallel β-sheet and a small piece of 3_{10}-helix. Comparison of the backbone of the apo(a) KIVT6 structure with the

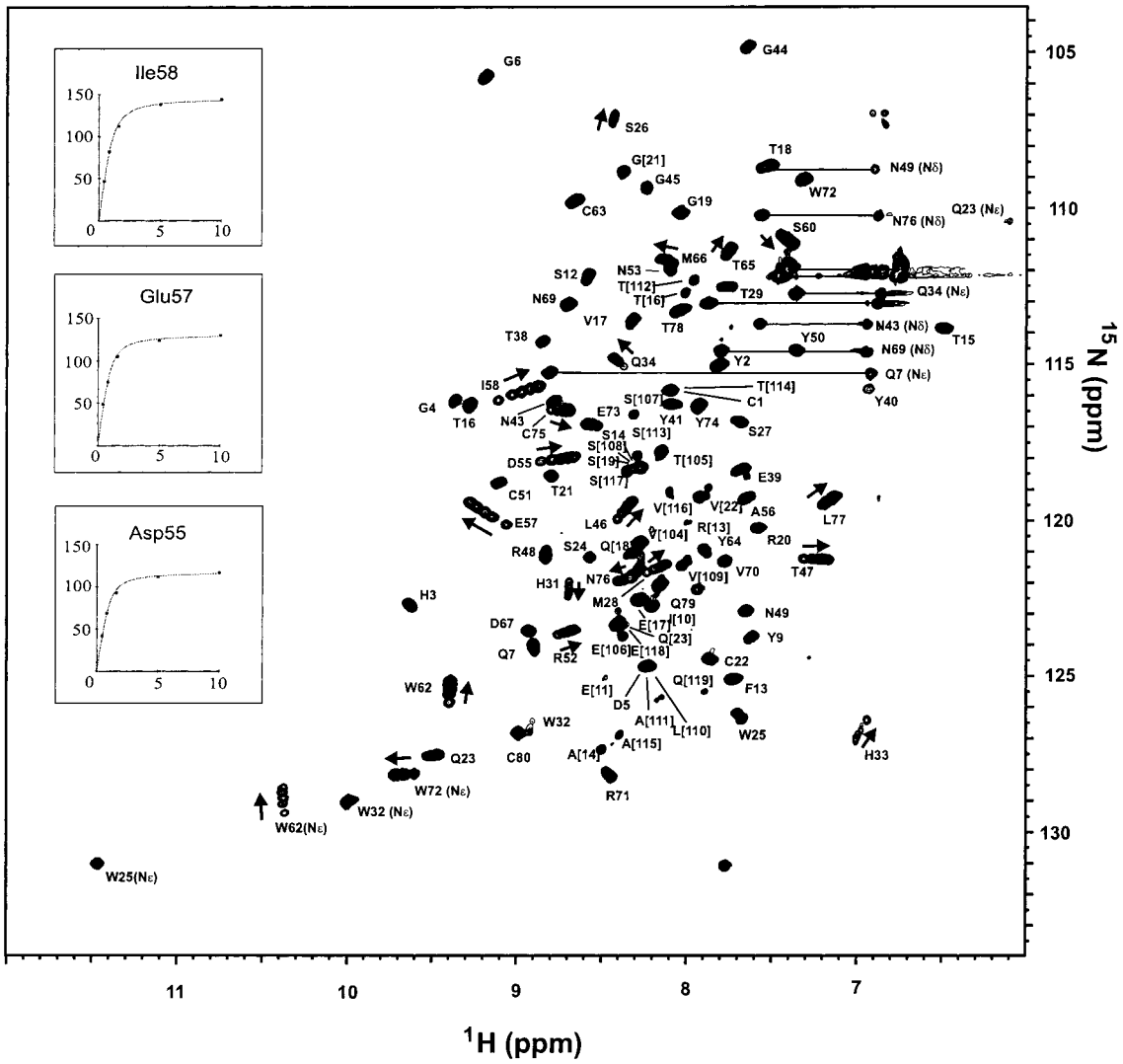

FIGURE 7: Overlaid 2D ^{1}H−^{15}N HSQC spectra from a titration of apo(a) KIVT6 with EACA. Arrows mark the direction of the main chemical shift perturbations. The *Y*-axis dimensions of the insets indicate the ^{1}H chemical shift perturbation in hertz. Residue numbering is according to the kringle convention. Numbers in brackets [*x*] refer to the full-length protein. The total EACA concentration is given on the *X*-axis. Data points were fitted with the program xcrvfit.

closest homologous crystal structures, apo(a) KIVT7, apo(a) KIVT10, and plasminogen K4, revealed a similar backbone folding and the existence of a similarly shaped lysine binding pocket.

A unique network of hydrogen bonds, involving the residues corresponding to Arg35, Tyr41, Asp55, and Tyr64, has been reported to occur in the crystal structure of KIVT7 (*20*). From our solution structure model of KIVT6 the existence of hydrogen bonds between Tyr41, Asp55, and Tyr64 in KIVT6 can be excluded. The absence of signals from the amide protons of Arg35 and Thr37 in the ^{1}H−^{15}N HSQC spectra indicates a high flexibility, which implies that these residues can hardly be engaged in strong hydrogen-bonding interactions.

Until now it has been argued that subtle structural differences within the LBS mediate the ligand fine specificity and the specificity in protein−kringle recognition (*20*, *53*). It is likely, however, that for protein−kringle recognition additionally an extended surface area on the kringle domain may be also important as hypothesized first by Cox et al. (*22*). For example the Arg32 in the plasminogen K4 sequence has been shown to be necessary for the binding to tetranectin (*71*). The character of this residue, which lies nearby but outside the LBS, might also be of particular importance in the protein−protein recognition properties of the kringle domains of apo(a). This can be inferred from the side chain orientation of Trp32 in apo(a) KIVT6, which closely resembles the orientation of the Arg32 side chain in apo(a) KIVT10 and plasminogen K4. Despite the hydrophobic character of this amino acid it is orientated toward the solvent and possesses a considerable flexibility. A similar result was concluded from NMR spectroscopic investigations of equine plasminogen K4 (*22*), which comprises also a tryptophan residue at position 32. The Arg → Trp substitution at this position occurs in a uniform manner in apo(a) KIVT6−8, which are referred to contain the binding interface for the initial noncovalent interaction with apoB100 (*12*−*14*). This conservative exchange of amino acids might reflect similar functional properties of apo(a) KIVT6−8.

The presented solution structure of apo(a) KIVT6 provides new detailed insights in the fine structure of the LBS in apo(a) KIVT6 and may serve as an additional starting point for homology modeling studies. Furthermore, it should allow a better understanding of the ligand fine specificity

observed in apo(a) kringle domains. This might also lead to specific ligands for apo(a) KIVT6, which are potentially suitable as anti-hyperlipoprotein(a) drugs. The hydroxyl group of Tyr64 might be a good starting point, since it provides a hydrogen-bonding donor/acceptor activity within the LBS. This additional hydrogen-bonding donor/acceptor activity is probably also present in apo(a) KIVT7−8, because these kringle domains contain a tyrosine residue in the corresponding position but not in apo(a) KIVT10 or plasminogen K4 since the corresponding position is occupied by a phenylalanine residue. It is notably that equine plasminogen K4 (*22*) has also a sequence identity with apo(a) KIVT6 at position 64. The tyrosine side chain seems, compared with ref *22*, to possess a similar position in the kringle domain.

ACKNOWLEDGMENT

We thank Dr. F. Andreae (PiChem, Graz, Austria) for performing the RP-HPLC, Dr. T. Stockner and Dr. K. Zangger for computational support, and Dr. W. Keller for the CD spectra.

SUPPORTING INFORMATION AVAILABLE

One table giving the chemical shifts of the full-length apo(a) KIVT6 resulting from the sequence-specific assignment (residue numbering is according to the full-length protein). This material is available free of charge via the Internet at http://pubs.acs.org.

REFERENCES

1. Berg, K. (1963) *Acta Pathol. Microbiol. Scand. 59*, 369−382.
2. Utermann, G. (1989) *Science 246*, 904−910.
3. McLean, J. W., Tomlinson, J. E., Kuang, W. J., Eaton, D. L., Chen, E. Y., Fless, G. M., Scanu, A. M., and Lawn, R. M. (1987) *Nature 330*, 132−137.
4. Lawn, R. M. (1996) *Clin. Genet. 49*, 167−174.
5. Trexler, M., and Patthy, L. (1983) *Proc. Natl. Acad. Sci. U.S.A. 80*, 2457−2461.
6. Magnusson, S., Sottrup-Jensen, L., Petersen, T. E., Dudek-Wojciechowska, G., and Claeys, H. (1976) in *Ribbons DW, Proteolysis and physiological regulation* (Brew, K., Ed.) Academic Press, New York.
7. McMullen, B. A., and Fujikawa, K. (1985) *J. Biol. Chem. 260*, 5328−5341.
8. van Zonneveld, A. J., Veerman, H., MacDonald, M. E., van Mourik, J. A., and Pannekoek, H. (1986) *J. Cell. Biochem. 32*, 169−178.
9. Gunzler, W. A., Steffens, G. J., Otting, F., Kim, S. M., Frankus, E., and Flohe, L. (1982) *Hoppe Seyler's Z. Physiol. Chem. 363*, 1155−1165.
10. Nakamura, T., Nishizawa, T., Hagiya, M., Seki, T., Shimonishi, M., Sugimura, A., Tashiro, K., and Shimizu, S. (1989) *Nature 342*, 440−443.
11. Trexler, M., and Patthy, L. (1984) *Biochim. Biophys. Acta 787*, 275−280.
12. Gabel, B. R., and Koschinsky, M. L. (1998) *Biochemistry 37*, 7892−7898.
13. Frank, S., and Kostner, G. M. (1997) *Protein Eng. 10*, 291−298.
14. Frank, S., Durovic, S., and Kostner, G. M. (1994) *Biochem. J. 304*, 27−30.
15. Keesler, G. A., Li, Y., Skiba, P. J., Fless, G. M., and Tabas, I. (1994) *Arterioscler. Thromb. 14*, 1337−1345.
16. Klezovitch, O., Edelstein, C., and Scanu, A. M. (1996) *J. Clin. Invest. 98*, 185−191.
17. Ernst, A., Helmhold, M., Brunner, C., Petho-Schramm, A., Armstrong, V. W., and Muller, H. J. (1995) *J. Biol. Chem. 270*, 6227−6234.
18. Guevara, J., Jr., Jan, A. Y., Knapp, R., Tulinsky, A., and Morrisett, J. D. (1993) *Arterioscler. Thromb. 13*, 758−770.
19. Hrzenjak, A., Frank, S., Maderegger, B., Sterk, H., and Kostner, G. M. (2000) *Protein Eng. 13*, 661−666.
20. Ye, Q., Rahman, M. N., Koschinsky, M. L., and Jia, Z. (2001) *Protein Sci. 10*, 1124−1129.
21. Mikol, V., LoGrasso, P. V., and Boettcher, B. R. (1996) *J. Mol. Biol. 256*, 751−761.
22. Cox, M., Schaller, J., Boelens, R., Kaptein, R., Rickli, E., and Llinas, M. (1994) *Chem. Phys. Lipids 67−68*, 43−58.
23. Mulichak, A. M., Tulinsky, A., and Ravichandran, K. G. (1991) *Biochemistry 30*, 10576−10588.
24. Atkinson, R. A., and Williams, R. J. (1990) *J. Mol. Biol. 212*, 541−552.
25. Bolotina, I. A., Chekhov, V. O., Lugauskas, V. I., Finkel'shtein, A. V., and Ptitsyn, O. B. (1980) *Mol. Biol. 14*, 891−902.
26. Marion, D., and Wuthrich, K. (1983) *Biochem. Biophys. Res. Commun. 113*, 967−974.
27. Wishart, D. S., Bigam, C. G., Yao, J., Abildgaard, F., Dyson, H. J., Oldfield, E., Markley, J. L., and Sykes, B. D. (1995) *J. Biomol. NMR 6*, 135−140.
28. Grzesiek, S., and Bax, A. (1992) *J. Magn. Reson. 96*, 432−440.
29. Schleucher, J., Sattler, M., and Griesinger, C. (1993) *Angew. Chem., Int. Ed. 32*, 1489−1491.
30. Kay, L. E., Xu, G. Y., and Yamazaki, T. (1994) *J. Magn. Reson. 109*, 129−133.
31. Muhandiram, D. R., and Kay, L. E. (1994) *J. Magn. Reson. 103*, 203−216.
32. Kay, L. E., Xu, G. Y., Singer, A. U., Muhandiram, D. R., and Forman-Kay, J. D. (1993) *J. Magn. Reson. 101*, 333−357.
33. Palmer, A. G., III, Cavanagh, J., Wright, P. E., and Rance, M. (1991) *J. Magn. Reson. 93*, 151−170.
34. Kay, L. E., Keifer, P., and Saarinen, T. (1992) *J. Am. Chem. Soc. 114*, 10663−10665.
35. Schleucher, J., Schwendinger, M., Sattler, M., Schmidt, P., Schedletzky, O., Glaser, S. J., Sorensen, O. W., and Griesinger, C. (1994) *J. Biomol. NMR 4*, 301−306.
36. Vuister, G. W., and Bax, A. (1994) *J. Biomol. NMR 4*, 193−200.
37. Delaglio, F., Grzesiek, S., Vuister, G. W., Zhu, G., Pfeifer, J., and Bax, A. (1995) *J. Biomol. NMR 6*, 277−293.
38. Kraulis, P. J., Domaille, P. J., Campbell-Burk, S. L., Van Aken, T., and Laue, E. D. (1994) *Biochemistry 33*, 3515−3531.
39. Kraulis, P. J. (1989) *J. Magn. Reson. 84*, 627−633.
40. Kumar, A., Wagner, G., Ernst, R. R., and Wuthrich, K. (1981) *J. Am. Chem. Soc. 103*, 3654−3658.
41. Hyberts, S. G., Goldberg, M. S., Havel, T. F., and Wagner, G. (1992) *Protein Sci. 1*, 736−751.
42. Wuthrich, K., Billeter, M., and Braun, W. (1983) *J. Mol. Biol. 169*, 949−961.
43. Pardi, A., Billeter, M., and Wuthrich, K. (1984) *J. Mol. Biol. 180*, 741−751.
44. Cornilescu, G., Delaglio, F., and Bax, A. (1999) *J. Biomol. NMR 13*, 289−302.
45. Bruenger, A. T. (1992) *X-PLOR (Version 3.0) Manual: A System for Crystallography and NMR*, Yale University, New Haven, CT.
46. Brooks, B. R., Bruccoleri, R. E., Olafson, B. D., States, D. J., Swaminathan, S., and Karplus, M. (1983) *J. Comput. Chem. 4*, 187−217.
47. Nilges, M., Clore, G. M., and Gronenborn, A. M. (1988) *FEBS Lett. 229*, 317−324.
48. Greenfield, N., and Fasman, G. D. (1969) *Biochemistry 8*, 4108−4116.
49. Chen, Y. H., Yang, J. T., and Chau, K. H. (1974) *Biochemistry 13*, 3350−3359.
50. Yang, J. T., Wu, C. S., and Martinez, H. M. (1986) *Methods Enzymol. 130*, 208−269.

51. Hansen, A. P., Petros, A. M., Meadows, R. P., Nettesheim, D. G., Mazar, A. P., Olejniczak, E. T., Xu, R. X., Pederson, T. M., Henkin, J., and Fesik, S. W. (1994) *Biochemistry 33*, 4847−4864.
52. Mathews, I. I., Vanderhoff-Hanaver, P., Castellino, F. J., and Tulinsky, A. (1996) *Biochemistry 35*, 2567−2576.
53. Marti, D. N., Schaller, J., and Llinas, M. (1999) *Biochemistry 38*, 15741−15755.
54. de Vos, A. M., Ultsch, M. H., Kelley, R. F., Padmanabhan, K., Tulinsky, A., Westbrook, M. L., and Kossiakoff, A. A. (1992) *Biochemistry 31*, 270−279.
55. Mochalkin, I., Cheng, B., Klezovitch, O., Scanu, A. M., and Tulinsky, A. (1999) *Biochemistry 38*, 1990−1998.
56. McKay, R. T., Tripet, B. P., Hodges, R. S., and Sykes, B. D. (1997) *J. Biol. Chem. 272*, 28494−28500.
57. Marti, D. N., Hu, C. K., An, S. S., von Haller, P., Schaller, J., and Llinas, M. (1997) *Biochemistry 36*, 11591−11604.
58. Menhart, N., Sehl, L. C., Kelley, R. F., and Castellino, F. J. (1991) *Biochemistry 30*, 1948−1957.
59. Lerch, P. G., Rickli, E. E., Lergier, W., and Gillessen, D. (1980) *Eur. J. Biochem. 107*, 7−13.
60. Marti, D., Schaller, J., Ochensberger, B., and Rickli, E. E. (1994) *Eur. J. Biochem. 219*, 455−462.
61. McCance, S. G., Menhart, N., and Castellino, F. J. (1994) *J. Biol. Chem. 269*, 32405−32410.
62. Rejante, M. R., Byeon, I. J., and Llinas, M. (1991) *Biochemistry 30*, 11081−11092.
63. Sehl, L. C., and Castellino, F. J. (1990) *J. Biol. Chem. 265*, 5482−5486.
64. Chang, Y., Mochalkin, I., McCance, S. G., Cheng, B., Tulinsky, A., and Castellino, F. J. (1998) *Biochemistry 37*, 3258−3271.
65. Thewes, T., Constantine, K., Byeon, I. J., and Llinas, M. (1990) *J. Biol. Chem. 265*, 3906−3915.
66. Kelley, R. F., DeVos, A. M., and Cleary, S. (1991) *Proteins 11*, 35−44.
67. Byeon, I. J., Kelley, R. F., Mulkerrin, M. G., An, S. S., and Llinas, M. (1995) *Biochemistry 34*, 2739−2750.
68. Rejante, M. R., and Llinas, M. (1994) *Eur. J. Biochem. 221*, 939−949.
69. Wu, T. P., Padmanabhan, K., Tulinsky, A., and Mulichak, A. M. (1991) *Biochemistry 30*, 10589−10594.
70. Byeon, I. J., and Llinas, M. (1991) *J. Mol. Biol. 222*, 1035−1051.
71. Graversen, J. H., Sigurskjold, B. W., Thogersen, H. C., and Etzerodt, M. (2000) *Biochemistry 39*, 7414−7419.
72. Laskowski, R. A., MacArthur, M. W., Moss, D. S., and Thornton, J. M. (1993) *J. Appl. Crystallogr. 26*, 283−291.
73. Koradi, R., Billeter, M., and Wuthrich, K. (1996) *J. Mol. Graphics 14*, 51−55, 29−32.

BI011430K